Solar Energy Materials & Solar Cells 240 (2022) 111723

Contents lists available at ScienceDirect

Solar Energy Materials and Solar Cells

journal homepage: www.elsevier.com/locate/solmat

Sub-ambient radiative cooling under tropical climate using highly reflective polymeric coating

Di Han [a,1], Jipeng Fei [a,1], Jyotirmoy Mandal [b], Zhixin Liu [a], Hong Li [a], Aaswath P. Raman [b], Bing Feng Ng [a,*]

[a] School of Mechanical and Aerospace Engineering, Nanyang Technological University, 50 Nanyang Avenue, Singapore, 639798
[b] Department of Materials Science and Engineering, University of California, Los Angeles, CA, USA

ARTICLE INFO

Keywords:
Sub-ambient radiative cooling
Polymeric coating
Mie scattering
Solar reflectance
Tropical climate

ABSTRACT

While passive radiative cooling has shown great potential in temperate regions in lowering surface temperatures, its cooling performance under tropical climate that is characterised by high solar irradiance and humidity still lacks exploration. Herein, we adopt a highly reflective polymeric coating with $BaSO_4$ particles dispersed in P (VdF-HFP) matrix for radiative cooling in the tropics. Through the strong Mie scattering of sunlight and intrinsic bond vibration, the substrate-independent average solar reflectance and infrared emittance within the 8–13 μm atmospheric window could reach 97% and 94.2%, respectively. For the first time, surfaces could maintain sub-ambient temperatures under direct exposure to the sky and surroundings even when the solar intensity was 1000 W/m^2 and downwelling atmospheric radiation was 480 W/m^2, while separately achieving 2 °C below ambient during night-time with an effective cooling power of 54.4 W/m^2. With a scalable fabrication-process, our cost-effective single-layer coating can be easily applied to diverse substrates, which is suitable for real-world applications in the tropics.

1. Introduction

The increase in energy demand for cooling has become a global challenge in the 21st century, especially for countries with tropical climate [1]. Conventional cooling methods, such as air-conditioning and mechanical ventilation systems, consume large amounts of electrical energy and dump undesired greenhouse gases into the atmosphere that exacerbates global warming [2]. On the other hand, passive radiative cooling provides a zero-energy solution by releasing excessive heat to outer space through the atmospheric window (8–13 μm) [3,4]. Early works have demonstrated that effective radiative cooling can be achieved at night using selective or broadband emitters [5–8]. Driven by significant progress in the development of radiative cooling materials with strong solar reflectance, daytime radiative cooling has also picked up momentum recently [9,10]. Attempts have been made to design and fabricate photonic multilayer thin film with inorganic materials (Al_2O_3, Si_3N_4, SiO_2, Al and Si) [11–15]. Meanwhile, polymer membrane, aerogel cover and fabric textile have proven to be easily-processable materials for large-scale applications [16–22]. Moreover, cost-effective coatings or paints can be applied on diverse surfaces, which is highly desired for real-world applications [23–26].

While radiative cooling has shown to be highly effective in temperate regions, daytime radiative cooling under subtropical and tropical climate remains a challenge given the high solar energy, humidity and ambient temperature that can significantly affect cooling performances [27,28]. For instance, an efficient radiative cooler proposed in California that readily reached sub-ambient surface temperatures [10] does not work well in Singapore and Hong Kong [28,29]. In another study conducted in Hong Kong [30], effective cooling could not be achieved under direct sunlight even with an average solar reflectance of 95% and emittance of 98% within the 8–13 μm wavelength. Similarly, the surface temperature of a coating with 90.7% reflectance over the solar spectrum and 90.1% emittance in the atmospheric window was 3–10 °C above ambient temperature in hot and humid weather in Shanghai [31].

The main differences between tropical and temperate climates are the characteristics and amount of solar irradiance [32]. In our recent investigation [28], the composition of ultraviolet (UV) and visible light (VIS) within the solar spectrum is higher for the tropics than the

* Corresponding author.
E-mail address: bingfeng@ntu.edu.sg (B.F. Ng).
[1] These authors contributed equally to this work.

https://doi.org/10.1016/j.solmat.2022.111723
Received 11 January 2022; Received in revised form 3 March 2022; Accepted 21 March 2022

temperate region (AM 1.5 [33], which corresponds to a tilted surface at 37° with a solar zenith angle of 48° and reflects the average of 48 contiguous states of the US), as shown in Fig. 1a. The difference can be larger when the sample surface in midlatitude area is not facing the sun with a total solar power of 900 W/m^2. As a result, one of the key determining factors for radiative coolers to be effective in the tropics is to possess high reflectance in the solar spectrum, especially in the UV and VIS range. However. conventional reflective materials for radiative cooling have undesired solar absorption in the UV range that can restrain cooling performances [12,17,31].

The performance of radiative cooling is also highly influenced by the effects of humidity and ambient temperature under different climatic conditions [28,34,35]. Theoretical investigations on two cities in Australia indicated that cooling performances were poorer for the same radiative cooler under higher humidity levels [3]. Similar observation was also made through experiments where obvious drop in cooling power of 86.6 W/m^2 was found as total precipitable water was increased [35]. In another study, surface temperatures of radiative cooler in spring was about 6 °C below ambient, while that in summer was only 2.7 °C during daytime with clear skies [36]. Evidently, the increased downwelling atmospheric radiation induced by higher humidity and ambient temperature in the tropical climate has the potential to almost halve the amount of cooling power (from 140 W/m^2 to 70 W/m^2), as shown in Fig. 1a. The cooling power will drop to around 50 W/m^2 with the increased atmospheric radiation at larger zenith angle when considering the whole hemispherical plane [4]. Consequently, to achieve sub-ambient cooling in the tropical climate, further improvements to present materials are required to reduce solar absorption (especially in the UV range) and to increase infrared emission within the atmospheric window.

In this work, we propose the use of a highly solar-reflective coating with barium sulfate ($BaSO_4$) particles dispersed in P(VdF-HFP) polymeric network for passive radiative cooling under the tropical climate [25]. The efficient Mie scattering from broad particle size distribution and limited solar absorption of $BaSO_4$ enable a high substrate-independent solar reflectance of 97%. Besides, the average emittance within 8–13 μm wavelength is around 94.2%, induced by intrinsic bond vibrations of P(VdF-HFP) and $BaSO_4$. By taking advantage of the radiative cooling mechanism as shown in Fig. 1b, the scalable single-layer coating could approach sub-ambient temperatures under a solar radiation intensity of 1000 W/m^2, and up to 2 °C below ambient temperatures during night-time in the hot and humid conditions of Singapore, yielding an effective cooling power of 54.4 W/m^2. Furthermore, the low-cost BP [$BaSO_4$–P(VdF-HFP)] coating with general fabrication method also exhibits hydrophobicity, good flexibility, strong mechanical strength, and durability for rainy season, which are favourable characteristics for many applications. Our experimental and theoretical findings provide promising opportunities to achieve cooling in the tropics through the carefully designed radiative coatings.

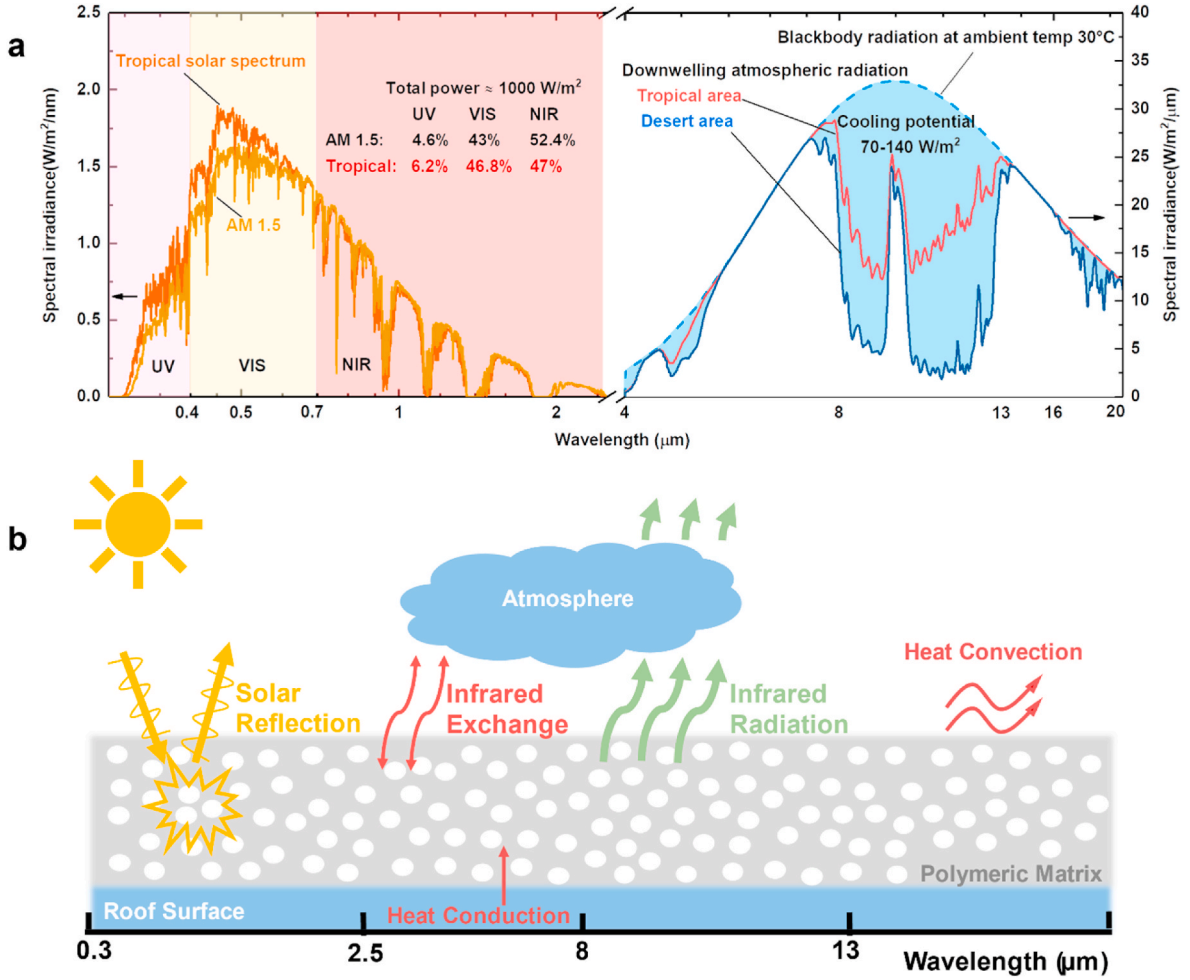

Fig. 1. Solar spectrum, atmospheric radiation and mechanics of radiative cooling. (a) Simulated solar spectrum and downwelling atmospheric radiation at 0° zenith angle under different climates (The solar spectrum was simulated using SMARTS [37] and the atmospheric radiation was modeled using Eq. (3) in Section 3.). (b) Cooling of surface through the mechanisms of solar reflection and infrared radiation across the atmospheric window.

2. Experiment

2.1. Materials and methods

The experimental work to demonstrate radiative cooling in the tropics involves a rooftop experiment to capture temperature of the BP coating under both daytime and night-time. Here, the experimental procedure is introduced where a description of the BP coating fabrication is first presented, followed by the methodology for the measurement of cooling performance. Lastly, the methodology for the characterization of material is described.

2.1.1. BP coating fabrication

To achieve high solar reflectance, $BaSO_4$ was selected for its high UV-reflectance [38] and was dispersed into P(VdF-HFP) matrix. BP coating was fabricated through a sol-gel method by solvent removal as shown in Fig. 2a. $BaSO_4$ powder (Sigma-Aldrich) was first grinded, followed by dispersion in NMP with stirring and sonication to obtain a uniform $BaSO_4$ solution. P(VdF-HFP) pellet was then dissolved in an acetone/NMP mixed solvent at 80 °C for 2 h. The mass ratio of P(VdF-HFP) and $BaSO_4$ is 1:6. The BP coating precursor was subsequently obtained by mixing the two solutions together, which was then coated onto a polished aluminium plate for solvent evaporation. The free-standing BP coating was then peeled off after the removal of acetone and NMP with 60 °C heating.

2.1.2. Temperature and cooling power measurements

To investigate the cooling performance of BP sample under tropical climate, we performed continuous outdoor measurements for steady-state temperature and cooling power on the rooftop of Academic Block North in Nanyang Technological University, Singapore (1.34° N, 103.68° E). The cross-section schematic of the set-up for temperature and cooling power measurements on the rooftop is shown in Fig. 2b. To minimise heat conduction, the sample was supported by low heat conductivity EPS foam with the same cross-sectional area. The surface temperatures of samples were measured using K-type self-adhesive thermocouples (SA3-K-120, Omega). As shown in Fig. 2b, the thermocouple was attached to the centre of the sample at the bottom surface. The ambient air temperature and relative humidity were obtained from the weather station placed near the set-up. To avoid solar heating for the weather station, the K-type thermocouple probe and humidity sensor were placed inside a 12-ring solar radiation shield (Delta Ohm) with free air flow. The cooling power was measured using a polyimide film heater attached to the bottom surface of the sample. The heater was powered by a constant current source. The sum of direct and diffuse solar irradiance (global radiation) was measured using a secondary standard pyranometer (LP PYRA 10, Delta Ohm). The far infrared radiation (atmospheric radiation) was measured by a passive pyrgeometer (LP PYRG 01, Delta Ohm) The above data was acquired using NI Data acquisition (DAQ) input modules and registered by a laptop.

2.1.3. Optical, thermal and mechanical measurement

The solar reflectance of samples within the wavelengths of 0.3–2.5 μm was measured by a UV-VIS-NIR spectrometer (PerkinElmer-Lambda 950) with built-in 150 mm integrating sphere, using a certified Spectralon® diffuse reflectance standard (Labsphere). The averaged total solar reflectance was obtained based on AM 1 solar spectrum. The infrared reflectance for the wavelength between 2.5 and 20 μm was measured by a Fourier transform infrared spectrometer (PerkinElmer Spectrum 3) using a gold-coated integrating sphere (PIKE Mid-IR

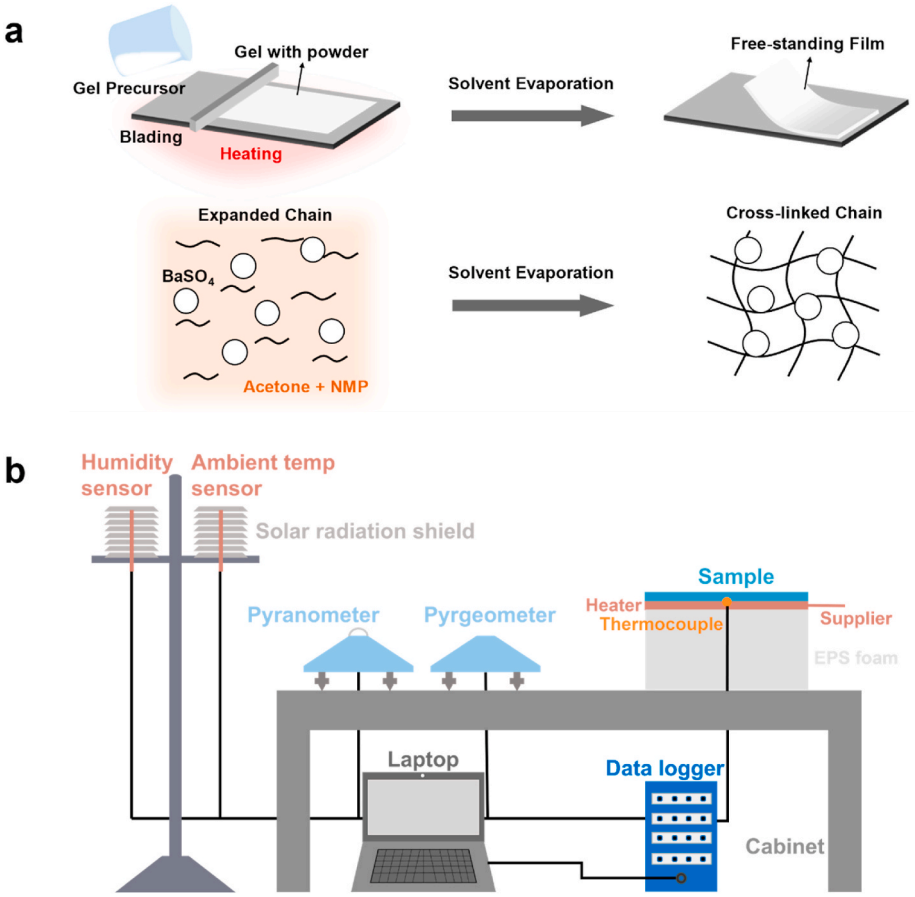

Fig. 2. BP coating fabrication and set-up for cooling performance. (a) Schematic of sol-gel fabrication process to achieve free-standing film of the BP coating. (b) Cross-section schematics of the set-up for cooling power and temperature (without the heater and power supply) measurements.

IntegratIR) with 8-degree incident angle. The SEM image was taken by a field-emission scanning electron microscope (JEOL 7600L). The contact angle of water was taken by a high-speed camera (Photron FASTCAM APX-RS). Infrared images were taken by a thermal imaging camera (FLIR E60). Optical images were photographed by HUAWEI HONOR 20pro. TGA, DSC tests were facilitated by TA Instruments- Q500 and Q200, respectively. Force-elongation curve was obtained by DEBEN Microtest 300N tensile stage.

3. Theoretical modelling

A theoretical model for cooling power and steady-state temperature is to be established to predict cooling performances of the BP coating based on data that is collected from the rooftop experiments. The governing equation of energy balance for the BP coating with surface temperature T_s under direct sunlight can be expressed as:

$$P_{cool}(T_s) = P_{rad}(T_s) - P_{atm}(T_{amb}) - P_{solar} - P_{conv+cond}(T_s, T_{amb}) \quad (1)$$

where P_{cool} is the net cooling power, P_{rad} is the power emitted out by the coating, P_{atm} is the absorbed power from downwelling atmospheric radiation, P_{solar} is the absorbed power from solar irradiance and $P_{conv+cond}$ is the power loss due to heat convection and conduction of the coating with surroundings.

From Eq. (1), P_{rad} can be resolved as follows

$$P_{rad}(T_s) = 2\pi \int_0^{\frac{\pi}{2}} sin\theta cos\theta \int_0^{\infty} I_B(T_s, \lambda)\varepsilon(\lambda, \theta) d\theta d\lambda \quad (2)$$

where $I_B(T_s, \lambda) = \frac{2hc^2}{\lambda^5} \frac{1}{e^{hc/\lambda k_B T_s} - 1}$ is the intensity of black-body radiation at the surface temperature by Planck's law. The variables h, c, λ, k_B are Planck's constant, velocity of light, wavelength and Boltzmann constant, respectively. $\varepsilon(\lambda, \theta)$ is the measured spectral emissivity of BP coating. Separately, for P_{atm}

$$P_{atm}(T_{amb}) = 2\pi \int_0^{\frac{\pi}{2}} sin\theta cos\theta \int_0^{\infty} I_B(T_{amb}, \lambda)\varepsilon_{atm}(\lambda, \theta)\varepsilon(\lambda, \theta) d\theta d\lambda \quad (3)$$

where T_{amb} represents ambient air temperature and $I_B(T_{amb}, \lambda) = \frac{2hc^2}{\lambda^5} \frac{1}{e^{hc/\lambda k_B T_{amb}} - 1}$ is the intensity of black-body radiation at ambient temperature T_{amb} by Planck's law. $\varepsilon_{atm}(\lambda, \theta)$ represents the atmospheric emissivity, which can be calculated using atmospheric transmittance $t(\lambda)$ given by $\varepsilon_{atm}(\lambda, \theta) = 1 - t(\lambda)^{1/cos\theta}$ [39]. $t(\lambda)$ can be modeled from software MODTRAN [40].

For P_{solar}, the expression is given by

$$P_{solar} = \int_0^{\infty} \varepsilon(\lambda, \theta_{solar}) I_{solar}(\lambda) d\lambda \quad (4)$$

where I_{solar} is local solar illumination. Separately, $P_{conv+cond}$ is expressed as

$$P_{conv+cond}(T_s, T_{amb}) = h_c(T_{amb} - T_s) \quad (5)$$

where h_c is the combined non-radiative heat transfer coefficient due to heat convection and conduction of the coating with ambient air and substrate. We used the empirical formula $h_c = 8.3 + 2.5v$ [41], where v is the wind speed, to calculate the combined heat transfer coefficient in an open system. According to the local wind speed, $h_c = 10$ W/m^{2}K.

In principle, the net cooling power obtained from Eq. (1) when $T_s = T_{amb}$ corresponds to effective cooling power. In addition, steady-state temperature for the BP coating can be obtained by setting $P_{cool} = 0$ in Eq. (1). To simulate the steady-state temperature, real time data for solar intensity and ambient temperature were employed as input parameters, together with the average wind speed. The equations are solved using MATLAB to obtain cooling power and steady-state temperature.

4. Results and discussion

In this section, the factors influencing the reflectance are first analysed, followed by the micro-structure and optical properties of the BP coating. Next, the cooling performance under tropical climates and field tests using coating on concrete are investigated. Last, stability characterization of the BP coating is introduced.

4.1. Mass ratio and thickness effects on solar reflectance

Within the BP coating, strong Mie scattering occurs at particle boundaries to achieve high solar reflection. Intrinsically, P(VdF-HFP) is optically transparent due to free bonding vibration within the visible range. Thus, the number of scattering interfaces is proportional to the relative amount of penetrated $BaSO_4$, which determines the total solar reflectance. As shown in Fig. 3a, increased reflection was observed with increase in mass ratio (P(VdF-HFP): $BaSO_4$), which saturated after a ratio of 1:5. The corresponding reflection spectrum for different mass ratios (Fig. 3b) further indicates that light was efficiently scattered by $BaSO_4$ particles, and insufficient scattering was the result of UV adsorption by polymeric chains (1:3, 1:4) [42]. Evidently, reflectance saturates around 97% for film thickness of 600–700 μm with mass ratio of 1:6 as shown in Fig. 3c–d.

4.2. Micro-structure and optical properties

The simple solution-based fabrication process has been described in Section 2. After solvent evaporation, the free-standing film was formed with a dense structure as shown in the SEM image in Fig. 4a, with inset indicating a broad particle diameter distribution, centred around 300–400 nm that is comparable with UV wavelength. Finite-difference time-domain (FDTD) simulation (details in Supplementary material, Note 1) was used to calculate the scattering efficiency of $BaSO_4$ particles as a function of diameter from 0.2 to 2 μm according to Mie theory. It was found that the particles can strongly scatter sunlight within 0.3–1 μm as shown in Fig. 4b, which accounts for the majority of solar energy. Owing to efficient Mie scattering from a broad diameter distribution (0.2–1 μm) and negligible solar absorption of $BaSO_4$, a high substrate-independent solar reflectance of 97% was obtained as shown in Fig. 4c, especially in the UV range. As a result, the addition of $BaSO_4$ to the optically transparent P(VdF-HFP) can significantly affect solar reflection of the BP coating due to improved scattering. Besides, light transmission could be eliminated by having sufficient stack of dispersed $BaSO_4$ particles in the polymeric matrix, achievable by having coating thickness above 300 μm (Fig. 3c–d). Moreover, both $BaSO_4$ and P(VdF-HFP) possess high infrared (IR) absorption, owing to SO_4 (1100–1200 cm^{-1}), C–F (1000–1400 cm^{-1}) and C–C (3300 cm^{-1}) intrinsic vibrations that lead to an average emittance of 94.2% within 8–13 μm [43,44].

4.3. Cooling performance under tropical climate

Under the extremely hot and humid environment in tropics, the high-level solar heat and downwelling atmospheric radiation induced by high ambient temperature and humidity are two dominant energy inputs for the radiative cooling in the tropics. However, as shown in Fig. 5a, the freestanding BP sample was still able to achieve sustained sub-ambient temperatures under the solar irradiance of 1000 W/m^2 and atmospheric radiation of 480 W/m^2 on a clear day. The average temperature difference was around 1.5 °C. When it comes to night-time as shown in Fig. 5b, the BP sample showed sustained sub-ambient temperatures ($\Delta T_{ave} = 2$ °C) without a wind shield, resulting in an effective cooling power of about 54.4 W/m^2, as depicted in Fig. 5c. Besides, the cooling

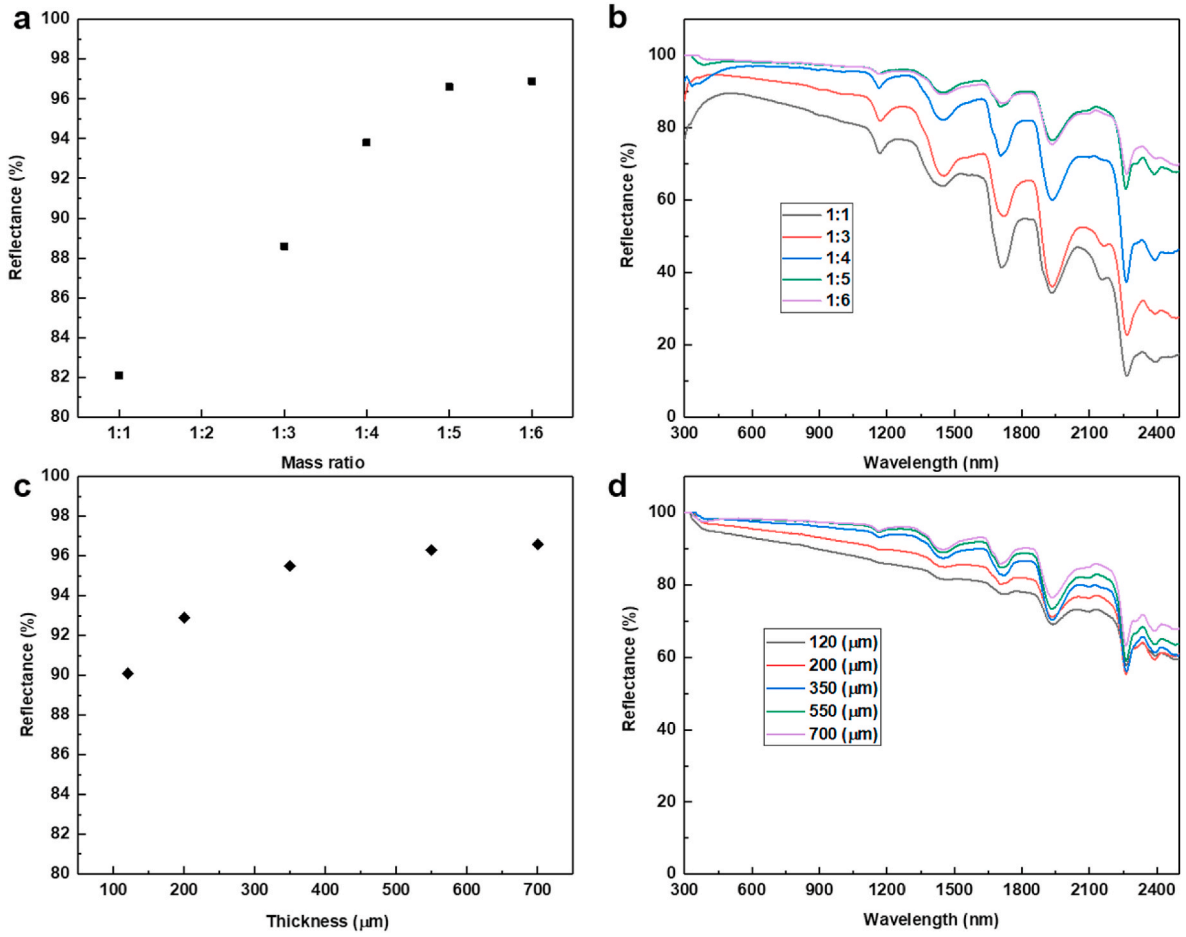

Fig. 3. Mass ratio and thickness effects on solar reflectance. (a) Solar reflectance variation with P(VdF-HFP):$BaSO_4$ mass ratios under controlled thickness of 700 μm. (b) Corresponding solar reflectance spectrums for different mass ratios. (c) Solar reflectance variation with thickness under controlled mass ratio of 1:6. (d) Corresponding solar reflectance spectrums for different thickness.

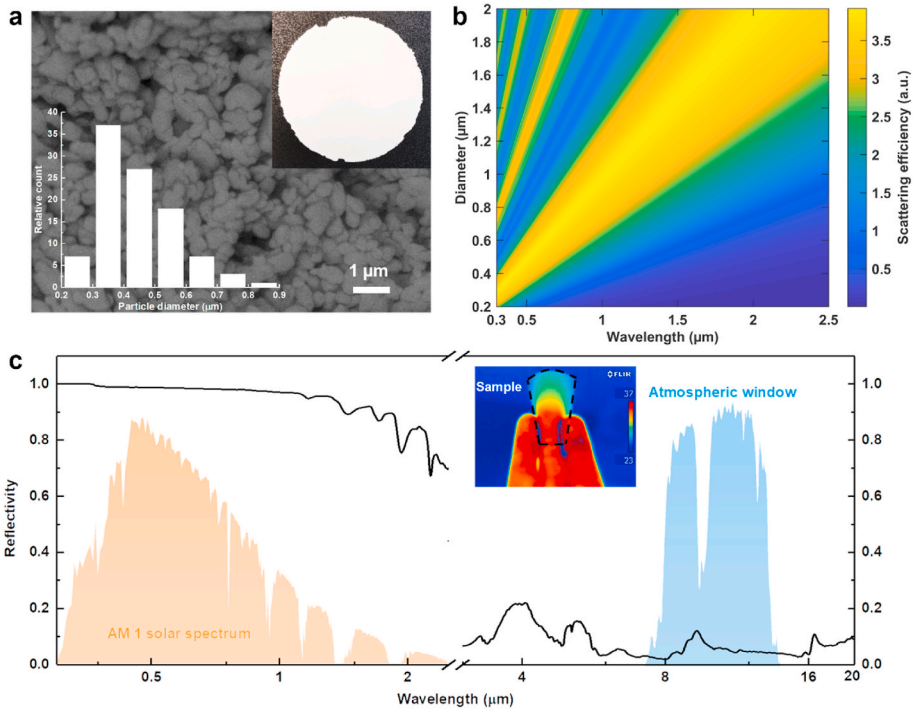

Fig. 4. Micro-structure and optical properties of BP coating. (a) SEM image of BP coating. Inset is optical image of the sample and particle size distribution. (b) FDTD simulation of scattering efficiency of $BaSO_4$ particles with diameter from 0.2 to 2 μm. (c) Measured spectral reflectivity of BP coating within 0.3–20 μm (Background is AM1 solar spectrum [45] (yellow) and atmospheric window (blue)). Inset is infrared image of the sample wrapped around fingers (The sample is partially in contact with the fingers). The colour of contacting part from IR view is almost the same as other fingers, which indicates high infrared emission compared with bare skin radiation.

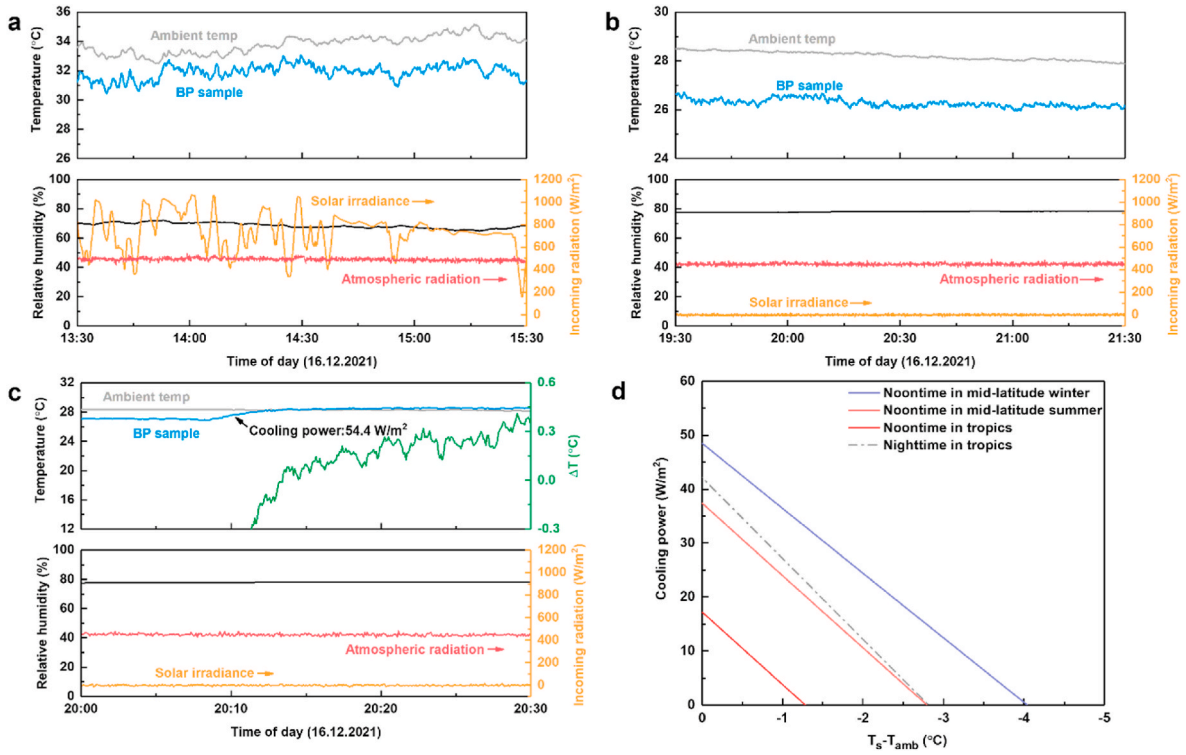

Fig. 5. Radiative cooling performances of BP sample (free-standing film with 700 μm thickness) under tropical climate in Singapore. (a) Measured daytime temperature on a clear day with corresponding humidity, solar irradiance and atmospheric radiation. (b) Measured night-time temperature on a clear night with corresponding humidity, solar irradiance and atmospheric radiation. (c) Measured night-time temperature on a clear night with corresponding humidity, solar irradiance and atmospheric radiation with heater turned on at time 20:08 for BP sample to match ambient temperatures for measurements of cooling power (54.4 W/m^2). (d) Simulated cooling power under different climates.

performance of BP sample in a closed chamber with wind shield can be found in Supplementary material, Note 2.

To further illustrate cooling performances under different climates, the net cooling power for BP sample was evaluated using the theoretical model and shown in Fig. 5d. The simulation conditions were summarized in Table 1. Owing to the high humidity levels (total water vapor column: TWC = 5119.4 atm-cm) in Singapore, the cooling performance during noontime under tropical climate was poorer than that in mid-latitude summer (TWC = 3635.9 atm-cm) under the same solar intensity of 1000 W/m^2 and ambient temperature of 35 °C. This difference could be larger if we consider reduced TWC levels of 1059.7 atm-cm in mid-latitude winter. The simulations reflected a cooling power of 17.2 W/m^2 at noontime in the tropics. Without the solar heat during nighttime, the simulated cooling power can be up to 42.1 W/m^2. In addition, the difference between the measured and simulated cooling power was analysed in Supplementary material, Note 3.

4.4. Field tests of BP coating on concrete

To further illustrate the applicability of BP material as a coating, field tests were conducted by directly coating BP onto concrete and comparing against commercial paint, with temperature measurements obtained through the insertion of thermocouples into the concrete, as shown in Fig. 6a. IR images of three different samples under direct sunlight can also be seen in Fig. 6a, where the surface temperature of BP coating was 4.7 °C lower than commercial coating, which was induced by the higher solar reflectance of BP coating, as displayed in Fig. 6b. Across the duration of measurements, the temperature of BP coating was about 4–8 °C lower than commercial coating as shown in Fig. 6c.

Table 1
Simulation conditions for different climates.

Climates	Humidity: total water vapor column (atm-cm)	Solar intensity (W/m^2)	Ambient temperature (°C)
Mid-latitude winter	1059.7	1000	10
Mid-latitude summer	3635.9	1000	35
Tropics	5119.4	1000	35

4.5. Stability characterization

A series of tests were conducted to investigate the stability of BP coating. Thermogravimetric analysis (TGA) results showed that water desorption and resided N-Methyl-2-pyrrolidone (NMP) (within bulk) (~46 °C and ~152 °C) led to continuous weight loss (Fig. 7a). P(VdF-HFP) and $BaSO_4$ exhibited excellent thermal stabilities within normal passive cooling conditions (<100 °C). From extensive evaluation, P(VdF-HFP) polymeric network was able to sustain up to 450 °C, while $BaSO_4$ remained stable at even higher temperature [46,47]. In addition, our free-standing BP coating shows good mechanical properties in stretching and twisting (Fig. 7b), with maximum tensile stress up to 4.42 MPa with 20% elongation. The good flexibility and strong mechanical strength suggest that the BP coating can be used for broad applications.

A reconstruction process was performed where the original sample (before reconstruction) was cut into pieces, and then dissolved in a solvent. A new free-standing film was made using the same method as the initial fabrication process. The spectral reflectance of the sample before and after reconstruction is depicted in Fig. 7c. The key parameter for radiative cooling (reflectance) remained almost the same after reconstruction, which indicated that the coating can be reused and recycled from the perspective of sustainability. In addition, the total solar reflectance variation of BP coating on concrete for 33 days of

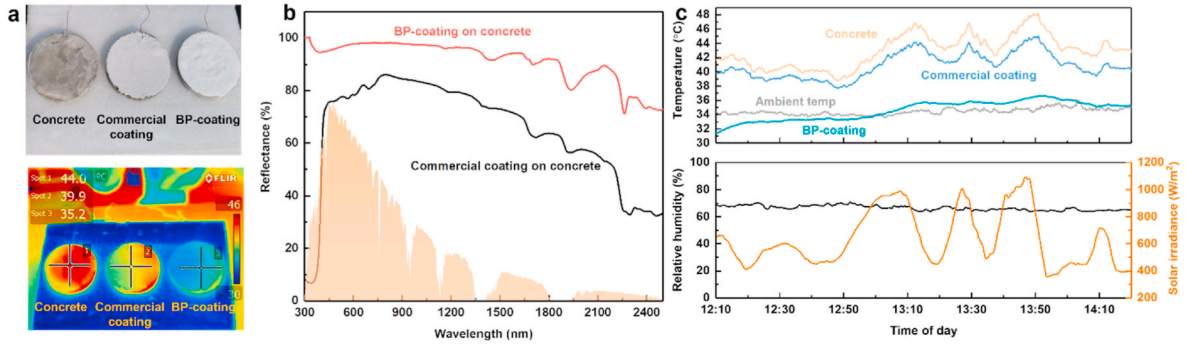

Fig. 6. Field tests of BP coating and commercial coating (NIPPON SOLAREFLECT Si) on concrete. (a) Optical image of three samples under direct sunlight (top). Infrared image of three samples on top of EPE (expanded polyethylene) foam under direct sunlight (bottom). The EPE foam showed a lower temperature as a result of the low infrared-emissivity of PE. (b) Spectral reflectance of BP coating and commercial coating on concrete. (c) Measured temperatures of coatings of same thickness against ambient temperature, with corresponding humidity and solar irradiance (wind speed: 0–3 m/s).

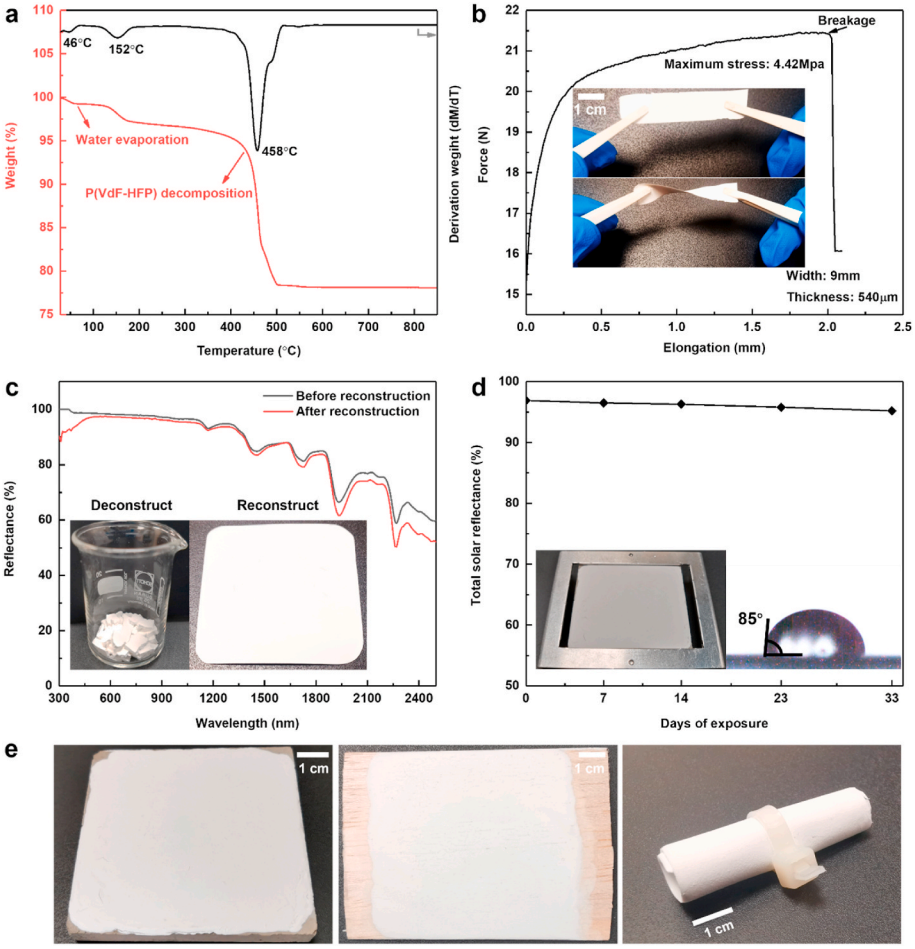

Fig. 7. Properties of BP coating. (a) TGA of BP coating. (b) Force-elongation curve for a 540 μm sample. Inset shows the stretching and twisting processes. (c) Spectral reflectance of the sample before and after reconstruction. Inset is optical image of pieces of sample (left) and free-standing film after reconstruction (right). As shown in insets, the original sample (before reconstruction) was cut into pieces, which were then dissolved in solvent. A new free-standing film was made using the same method as initial process. (d) Total solar reflectance variation of BP coating on concrete for 33 days of outdoor exposure in Singapore. Inset is optical image of exposed sample (left) and contact angle of water (right). The total solar reflectance of the exposed sample was measured indoors on the 1st, 7th, 14th, 23rd and 33rd day using the UV-VIS-NIR spectrometer. The duration of each measurement was only about 30 min and soon after, the sample was brought back for outdoor exposure on the rooftop. (e) Optical images of BP coating on different substrates. (left) Coating on concrete. (middle) Coating on wood. (right) Free-standing film.

outdoor exposure on the rooftop is shown in Fig. 7d. Owing to larger contact angle of water (shown from inset: 85°) compared with 57° measured from the commercial coating (NIPPON SOLAREFLECT Si), the total solar reflectance remained almost the same during a rainy season, which indicated durability for applications under the tropical climate. Furthermore, our BP coating can be made into free-standing film, or coating on diverse substrates such as concrete and wood, which is crucial for real applications as shown in Fig. 7e.

5. Conclusions

In conclusion, we adopt a highly solar-reflective coating with an average solar reflectance of 97% and thermal emittance of 94.2% within the 8–13 μm atmospheric window for passive radiative cooling under the tropical climate. For the first time, the scalable single-layer coating could approach sustained sub-ambient temperatures in the day and achieve up to 2 °C below ambient temperatures during night-time in hot and humid Singapore, yielding an effective cooling power of 54.4 W/m^2. Field tests on concrete showed that BP coating had lower surface temperatures (4–8 °C) as compared to commercial coating. Furthermore, the

difference between measured and simulated cooling power during night-time was analysed using the heat capacity of the material. The low-cost BP coating with easy fabrication also exhibited hydrophobicity, good flexibility, strong mechanical strength, and durability for rainy season, which are favourable for many applications in the tropical climate. Besides, our BP coating can be made into free-standing film, or coated onto diverse substrates such as concrete and wood, which is crucial for direct application.

CRediT authorship contribution statement

Di Han: Conceptualization, Data curation, Investigation, Writing – original draft. **Jipeng Fei:** Data curation, Investigation, Writing – original draft. **Jyotirmoy Mandal:** Investigation, Writing – review & editing. **Zhixin Liu:** Investigation. **Hong Li:** Resources, Writing – review & editing. **Aaswath P. Raman:** Investigation, Writing – review & editing. **Bing Feng Ng:** Conceptualization, Data curation, Supervision, Writing – review & editing.

Declaration of competing interest

The authors declare that they have no known competing financial interests or personal relationships that could have appeared to influence the work reported in this paper.

Acknowledgment

This study was funded by the Singapore Ministry of Education through grant no. 2018-T1-001-070.

Appendix A. Supplementary data

Supplementary data to this article can be found online at https://doi.org/10.1016/j.solmat.2022.111723.

References

[1] L. Pérez-Lombard, J. Ortiz, C. Pout, A review on buildings energy consumption information, Energy Build. 40 (3) (2008) 394–398, https://doi.org/10.1016/j.enbuild.2007.03.007.
[2] G.-R. Walther, E. Post, P. Convey, A. Menzel, C. Parmesan, T.J.C. Beebee, J.-M. Fromentin, O. Hoegh-Guldberg, F. Bairlein, Ecological responses to recent climate change, Nature 416 (6879) (2002) 389–395, https://doi.org/10.1038/416389a.
[3] M.M. Hossain, M. Gu, Radiative cooling: principles, progress, and potentials, Adv. Sci. 3 (7) (2016) 1500360, https://doi.org/10.1002/advs.201500360.
[4] D. Zhao, A. Aili, Y. Zhai, S. Xu, G. Tan, X. Yin, R. Yang, Radiative sky cooling: fundamental principles, materials, and applications, Appl. Phys. Rev. 6 (2) (2019), 021306.
[5] B. Bartoli, S. Catalanotti, B. Coluzzi, V. Cuomo, V. Silvestrini, G. Troise, Nocturnal and diurnal performances of selective radiators, Appl. Energy 3 (4) (1977) 267–286, https://doi.org/10.1016/0306-2619(77)90015-0.
[6] S. Catalanotti, V. Cuomo, G. Piro, D. Ruggi, V. Silvestrini, G. Troise, The radiative cooling of selective surfaces, Sol. Energy 17 (2) (1975) 83–89, https://doi.org/10.1016/0038-092X(75)90062-6.
[7] A. Hjortsberg, C.G. Granqvist, Radiative cooling with selectively emitting ethylene gas, Appl. Phys. Lett. 39 (6) (1981) 507–509, https://doi.org/10.1063/1.92783.
[8] D. Michell, K.L. Biggs, Radiation cooling of buildings at night, Appl. Energy 5 (4) (1979) 263–275, https://doi.org/10.1016/0306-2619(79)90017-5.
[9] E. Rephaeli, A. Raman, S. Fan, Ultrabroadband photonic structures to achieve high-performance daytime radiative cooling, Nano Lett. 13 (4) (2013) 1457–1461, https://doi.org/10.1021/nl4004283.
[10] A.P. Raman, M.A. Anoma, L. Zhu, E. Rephaeli, S. Fan, Passive radiative cooling below ambient air temperature under direct sunlight, Nature 515 (7528) (2014) 540–544, https://doi.org/10.1038/nature13883.
[11] Z. Chen, L. Zhu, A. Raman, S. Fan, Radiative cooling to deep sub-freezing temperatures through a 24-h day–night cycle, Nat. Commun. 7 (1) (2016) 13729, https://doi.org/10.1038/ncomms13729.
[12] J.-l. Kou, Z. Jurado, Z. Chen, S. Fan, A.J. Minnich, Daytime radiative cooling using near-black infrared emitters, ACS Photonics 4 (3) (2017) 626–630, https://doi.org/10.1021/acsphotonics.6b00991.
[13] D. Chae, M. Kim, P.-H. Jung, S. Son, J. Seo, Y. Liu, B.J. Lee, H. Lee, Spectrally selective inorganic-based multilayer emitter for daytime radiative cooling, ACS Appl. Mater. Interfaces 12 (7) (2020) 8073–8081, https://doi.org/10.1021/acsami.9b16742.
[14] M.M. Hossain, B. Jia, M. Gu, A metamaterial emitter for highly efficient radiative cooling, Adv. Opt. Mater. 3 (8) (2015) 1047–1051, https://doi.org/10.1002/adom.201500119.
[15] D. Wu, C. Liu, Z. Xu, Y. Liu, Z. Yu, L. Yu, L. Chen, R. Li, R. Ma, H. Ye, The design of ultra-broadband selective near-perfect absorber based on photonic structures to achieve near-ideal daytime radiative cooling, Mater. Des. 139 (2018) 104–111, https://doi.org/10.1016/j.matdes.2017.10.077.
[16] Y. Zhai, Y. Ma, S.N. David, D. Zhao, R. Lou, G. Tan, R. Yang, X. Yin, Scalable-manufactured randomized glass-polymer hybrid metamaterial for daytime radiative cooling, Science 355 (6329) (2017) 1062–1066, https://doi.org/10.1126/science.aai7899.
[17] A.R. Gentle, G.B. Smith, A subambient open roof surface under the mid-summer sun, Adv. Sci. 2 (9) (2015) 1500119, https://doi.org/10.1002/advs.201500119.
[18] T. Wang, Y. Wu, L. Shi, X. Hu, M. Chen, L. Wu, A structural polymer for highly efficient all-day passive radiative cooling, Nat. Commun. 12 (1) (2021) 365, https://doi.org/10.1038/s41467-020-20646-7.
[19] A. Leroy, B. Bhatia, C.C. Kelsall, A. Castillejo-Cuberos, H. Di Capua, L. Zhao, L. Zhang, A.M. Guzman, E.N. Wang, High-performance subambient radiative cooling enabled by optically selective and thermally insulating polyethylene aerogel, Sci. Adv. 5 (10) (2019), eaat9480, https://doi.org/10.1126/sciadv.aat9480.
[20] P.-C. Hsu, A.Y. Song, P.B. Catrysse, C. Liu, Y. Peng, J. Xie, S. Fan, Y. Cui, Radiative human body cooling by nanoporous polyethylene textile, Science 353 (6303) (2016) 1019–1023, https://doi.org/10.1126/science.aaf5471.
[21] D. Li, X. Liu, W. Li, Z. Lin, B. Zhu, Z. Li, J. Li, B. Li, S. Fan, J. Xie, J. Zhu, Scalable and hierarchically designed polymer film as a selective thermal emitter for high-performance all-day radiative cooling, Nat. Nanotechnol. 16 (2) (2021) 153–158, https://doi.org/10.1038/s41565-020-00800-4.
[22] K. Zhou, W. Li, B.B. Patel, R. Tao, Y. Chang, S. Fan, Y. Diao, L. Cai, Three-dimensional printable nanoporous polymer matrix composites for daytime radiative cooling, Nano Lett. 21 (3) (2021) 1493–1499, https://doi.org/10.1021/acs.nanolett.0c04810.
[23] J. Mandal, Y. Fu, A.C. Overvig, M. Jia, K. Sun, N.N. Shi, H. Zhou, X. Xiao, N. Yu, Y. Yang, Hierarchically porous polymer coatings for highly efficient passive daytime radiative cooling, Science 362 (6412) (2018) 315–319, https://doi.org/10.1126/science.aat9513.
[24] X. Xue, M. Qiu, Y. Li, Q.M. Zhang, S. Li, Z. Yang, C. Feng, W. Zhang, J.-G. Dai, D. Lei, W. Jin, L. Xu, T. Zhang, J. Qin, H. Wang, S. Fan, Creating an eco-friendly building coating with smart subambient radiative cooling, Adv. Mater. 32 (42) (2020) 1906751, https://doi.org/10.1002/adma.201906751.
[25] J. Mandal, Y. Yang, N. Yu, A.P. Raman, Paints as a scalable and effective radiative cooling technology for buildings, Joule 4 (7) (2020) 1350–1356, https://doi.org/10.1016/j.joule.2020.04.010.
[26] X. Li, J. Peoples, Z. Huang, Z. Zhao, J. Qiu, X. Ruan, Full daytime sub-ambient radiative cooling in commercial-like paints with high figure of merit, Cell Reports Physical Science 1 (10) (2020) 100221, https://doi.org/10.1016/j.xcrp.2020.100221.
[27] S.Y. Jeong, C.Y. Tso, J. Ha, Y.M. Wong, C.Y.H. Chao, B. Huang, H. Qiu, Field investigation of a photonic multi-layered TiO2 passive radiative cooler in sub-tropical climate, Renew. Energy 146 (2020) 44–55, https://doi.org/10.1016/j.renene.2019.06.119.
[28] D. Han, B.F. Ng, M.P. Wan, Preliminary study of passive radiative cooling under Singapore's tropical climate, Sol. Energy Mater. Sol. Cell. 206 (2020) 110270.
[29] C.Y. Tso, K.C. Chan, C.Y.H. Chao, A field investigation of passive radiative cooling under Hong Kong's climate, Renew. Energy 106 (2017) 52–61, https://doi.org/10.1016/j.renene.2017.01.018.
[30] S.Y. Jeong, C.Y. Tso, Y.M. Wong, C.Y.H. Chao, B. Huang, Daytime passive radiative cooling by ultra emissive bio-inspired polymeric surface, Sol. Energy Mater. Sol. Cell. 206 (2020) 110296, https://doi.org/10.1016/j.solmat.2019.110296.
[31] H. Bao, C. Yan, B. Wang, X. Fang, C.Y. Zhao, X. Ruan, Double-layer nanoparticle-based coatings for efficient terrestrial radiative cooling, Sol. Energy Mater. Sol. Cell. 168 (2017) 78–84, https://doi.org/10.1016/j.solmat.2017.04.020.
[32] R. Levinson, H. Akbari, P. Berdahl, Measuring solar reflectance—Part I: defining a metric that accurately predicts solar heat gain, Sol. Energy 84 (9) (2010) 1717–1744, https://doi.org/10.1016/j.solener.2010.04.018.
[33] Standard Tables for Reference Solar Spectral Irradiances: Direct Normal and Hemispherical on 37° Tilted Surface, ASTM International, West Conshohocken, PA, 2020.
[34] T. Suichi, A. Ishikawa, Y. Hayashi, K. Tsuruta, Performance limit of daytime radiative cooling in warm humid environment, AIP Adv. 8 (5) (2018), 055124, https://doi.org/10.1063/1.5030156.
[35] C. Liu, Y. Wu, B. Wang, C.Y. Zhao, H. Bao, Effect of atmospheric water vapor on radiative cooling performance of different surfaces, Sol. Energy 183 (2019) 218–225, https://doi.org/10.1016/j.solener.2019.03.011.
[36] J. Liu, D. Zhang, S. Jiao, Z. Zhou, Z. Zhang, F. Gao, Preliminary study of radiative cooling in cooling season of the humid coastal area, Sol. Energy Mater. Sol. Cell. 208 (2020) 110412, https://doi.org/10.1016/j.solmat.2020.110412.
[37] Smarts. https://www.nrel.gov/grid/solar-resource/smarts.html, 2022.
[38] J.B. Schutt, J.F. Arens, C.M. Shai, E. Stromberg, Highly reflecting stable white paint for the detection of ultraviolet and visible radiations, Appl. Opt. 13 (10) (1974) 2218–2221, https://doi.org/10.1364/AO.13.002218.
[39] C.G. Granqvist, A. Hjortsberg, Radiative cooling to low temperatures: general considerations and application to selectively emitting SiO films, J. Appl. Phys. 52 (6) (1981) 4205–4220, https://doi.org/10.1063/1.329270.
[40] Modtran, available from, http://modtran.spectral.com/modtran_home, 2020.

[41] D. Zhao, A. Aili, Y. Zhai, J. Lu, D. Kidd, G. Tan, X. Yin, R. Yang, Subambient cooling of water: toward real-world applications of daytime radiative cooling, Joule 3 (1) (2019) 111–123, https://doi.org/10.1016/j.joule.2018.10.006.
[42] L. Yesappa, M. Niranjana, S.P. Ashokkumar, H. Vijeth, M. Basappa, J. Dwivedi, V. C. Petwal, S. Ganesh, H. Devendrappa, Optical properties and ionic conductivity studies of an 8 MeV electron beam irradiated poly(vinylidene fluoride-co-hexafluoropropylene)/LiClO4 electrolyte film for opto-electronic applications, RSC Adv. 8 (28) (2018) 15297–15309, https://doi.org/10.1039/C8RA00970H.
[43] A. Gupta, P. Singh, C. Shivakumara, Synthesis of BaSO4 nanoparticles by precipitation method using sodium hexa metaphosphate as a stabilizer, Solid State Commun. 150 (9) (2010) 386–388, https://doi.org/10.1016/j.ssc.2009.11.039.
[44] P. Tuhania, P.K. Singh, B. Bhattacharya, P.S. Dhapola, S. Yadav, P. Shukla, M. Gupta, PVDF-HFP and 1-ethyl-3-methylimidazolium thiocyanate–doped polymer electrolyte for efficient supercapacitors, High Perform. Polym. 30 (8) (2018) 911–917, https://doi.org/10.1177/0954008318772009.
[45] Standard Table for Reference Solar Spectral Distributions: Direct and Diffuse on 20° Tilted and Vertical Surfaces, ASTM International, West Conshohocken, PA, 2014.
[46] W. Gao, Z. Wang, Z. Zhao, L. Ding, Y. Zhu, Effect of barium sulfate on thermal stability and crystallization properties of poly(ethylene terephthalate), J. Therm. Anal. Calorim. 129 (2) (2017) 1047–1055, https://doi.org/10.1007/s10973-017-6237-0.
[47] K. Polat, Energy harvesting from a thin polymeric film based on PVDF-HFP and PMMA blend, Appl. Phys. A 126 (7) (2020) 497, https://doi.org/10.1007/s00339-020-03698-w.